AFRL-OSR-VA-TR-2011-0400

Cooperative Communication For Tracking And Surveillance Using Multiple Related Observations And Distributed Transmitters

Zeger, Kenneth and Milstein, Laurence

The Regents of the University of California; University of California, San Diego

December 2010
Final Report

AIR FORCE RESEARCH LABORATORY
AF OFFICE OF SCIENTIFIC RESEARCH (AFOSR)/RSE
ARLINGTON, VIRGINIA 22203
AIR FORCE MATERIEL COMMAND

Report Documentation Page

Form Approved
OMB No. 0704-0188

1. REPORT DATE	2. REPORT TYPE	3. DATES COVERED
06 DEC 2010		**01-03-2006 to 30-11-2009**

4. TITLE AND SUBTITLE	5a. CONTRACT NUMBER
Cooperative Communication For Tracking And Surveillance Using Multiple Related Observations And Distributed Transmitters	5b. GRANT NUMBER
	5c. PROGRAM ELEMENT NUMBER
6. AUTHOR(S)	5d. PROJECT NUMBER
	5e. TASK NUMBER
	5f. WORK UNIT NUMBER
7. PERFORMING ORGANIZATION NAME(S) AND ADDRESS(ES)	8. PERFORMING ORGANIZATION REPORT NUMBER
The Regents of the University of California; University of California, San Diego,9500 Gilman Drive, Mail Code 0934,La Jolla,CA,92093-	**; AFRL-OSR-VA-TR-11-0400**
9. SPONSORING/MONITORING AGENCY NAME(S) AND ADDRESS(ES)	10. SPONSOR/MONITOR'S ACRONYM(S)
	11. SPONSOR/MONITOR'S REPORT NUMBER(S) **AFRL-OSR-VA-TR-11-0400**

12. DISTRIBUTION/AVAILABILITY STATEMENT
Approved for public release; distribution unlimited

13. SUPPLEMENTARY NOTES

14. ABSTRACT

15. SUBJECT TERMS

16. SECURITY CLASSIFICATION OF:			17. LIMITATION OF ABSTRACT	18. NUMBER OF PAGES	19a. NAME OF RESPONSIBLE PERSON
a. REPORT	b. ABSTRACT	c. THIS PAGE			
unclassified	**unclassified**	**unclassified**	**Same as Report (SAR)**	**11**	

AFOSR Final Report for 3-year funding at UCSD *

Laurence Milstein and Kenneth Zeger

Created: December 6, 2010 @ 10:56 am

* **L. Milstein and K. Zeger** are with the Department of Electrical and Computer Engineering, University of California, San Diego, La Jolla, CA 92093-0407 (milstein@ece.ucsd.edu, zeger@ucsd.edu).

Air Force Office of Scientific Research, Contract Number FA9550-06-1-0210, "*Cooperative Communication using Multiple Related Observations and Distributed Transmitters*".

1 OFDM Performance with Non-ideal Receivers

We studied the performance of OFDM with imperfections due to receiver non-idealities, such as residual timing error, residual frequency error and noisy channel estimates, as well as due to channel characteristics, such as Doppler and delay spread exceeding the OFDM symbol's cyclic prefix (CP). These non-ideal characterizations are key to be able to assess how well a cognitive receiver can work with different channel conditions. For example, at low SNRs, it may be better to operate with a lower CP overhead, since the performance is limited by thermal noise. Conversely, in very high SNR regimes, it may be better to incur more CP overhead and possible pilot overhead to exploit the channel capacity at the regime by reducing the interference and by improving the channel estimates. More specifically, we presented an OFDM model thoroughly characterizing the intersymbol interference (ISI) and intercarrier interference (ICI) terms. Different data detectors were formulated, and performance comparisons were presented.

A performance study specialized on ultrawideband systems (UWB) systems has also been shown to characterize the sensitivity of an OFDM-based UWB system to key system parameters. We analyzed the impact of realistic channel estimation in OFDM systems, accounting for imperfections such as residual time and frequency error, and a channel delay spread larger than the CP. The impact of the pilot signal density on the data demodulation performance was also studied. Among our results were the following: At different levels of residual frequency error, the effect of ICI on channel estimation has been shown to be small. However, ISI can severely impact the quality of the channel estimates, and hence can yield a large ($>$ 2dB) data demodulation performance degradation when compared to ideal channel estimation. The pilot signal density and the associated channel estimation algorithm were shown to be critical for the ISI cases. Note that ISI may be incurred by a channel delay spread larger than the CP, or by timing errors at the terminal receiver (late sampling), irrespective of the channel delay spread. The large degradation in performance due to ISI emphasizes the importance of selecting an adequate CP length in OFDM systems. Further, channel estimation algorithms providing robust performance in the presence of ISI are critical for robust performance of OFDM systems. Therefore, the framework presented in this work enables studies of various system trade-offs when designing OFDM systems, ranging from optimal values of OFDM system parameters such as symbol duration, T, number of subcarriers, N, and pilot overhead, to robustness against different receiver impairments, such as time and frequency synchronization errors.

The discrete-time OFDM transmit waveform at baseband is given by

$$u[n,k] = \frac{1}{\sqrt{N}} \sum_{m=-N/2}^{N/2-1} s[n,m] \cdot e^{j2\pi m(k-CP)/N} \cdot \Pi_s[\frac{k}{N_T}] \tag{1}$$

where N is the number of subcarriers, CP is the duration in samples of the CP, $N_T \triangleq (N+CP)$, and $s[n,m]$ are the information symbols, in general complex. The index n is used as a time index and refers to a particular OFDM symbol, the index m is used as a subcarrier index within the OFDM symbol, and the index k is used as a time index for samples within a given OFDM block. The OFDM symbol duration in seconds is $T \triangleq NT_c$, and the OFDM block duration is $T_f \triangleq N_T T_c$, where T_c is the symbol duration prior to the OFDM modulation. Finally, $\Pi_s[k/N_T]$ is the shifted

rectangular function with unit amplitude and spans the interval $k \in [0, N_T - 1]$.

The transmitter gives an analog support to the discrete-time signal $u[n,k]$ by way of a digital-to-analog conversion (DAC) or pulse shaping filter that we denote by $h^{tx}(t)$, yielding

$$x_{lp}(t) = \sum_n \sum_k^{N_T-1} u[n,k] h^{tx}(t - kT_c - nT_f), \tag{2}$$

which will be up-converted to the carrier frequency, f_0. Note that we will denote the locally generated carrier frequency at the OFDM transmitter by $\hat{f}_0$.

2 Effects of Imperfections on the Performance of OFDM Systems

The results assume a system with a subcarrier spacing of 4.125MHz, *N*=128 subcarriers, and a Nyquist filter with 0% roll-off and bandwidth 528MHz. Note that CP durations of 0, 16, 32, 48, 64, and 80 samples constitute 0%, 11.11%, 20%, 27.27%, 33.33%, and 38.46% fixed overhead. The results shown in Figures 1 and 2 assume perfect time and frequency synchronization, an MF receiver, and result from averaging the performance over 1000 channel realizations. Note that for both of the channel models, at some point a longer CP does not improve the performance; this is the point where the ISI is not significant.

Figure 1 shows the sensitivity to frequency errors for a given line-of-sight channel realization. The results are obtained assuming a system with *N*=128, 20% CP overhead, perfect time synchronization, a Nyquist filter with 0% roll-off and a bandwidth of 528MHz, and an MF receiver. This figure contains analytical (distinguished by lines with inserted characters, e.g., '-*-') and simulation based (distinguished by just characters, e.g., '*') results for frequency errors ranging from 0 to 5% of the subcarrier frequency spacing. Assuming a $\pm$20ppm frequency tolerance at the transmitter and at the receiver, the maximum frequency error incurred would be $\pm$40ppm, which for a 5GHz carrier frequency and 4.125MHz subcarrier spacing equates to a frequency error of 5% of the subcarrier spacing. Note that the frequency error in actual systems would typically be compensated by some frequency compensation mechanism, so that these results show the performance at different levels of residual frequency error. From the results, we can see a graceful performance degradation as frequency errors increase.

Figure 2 shows the sensitivity to timing errors. The same assumptions as for the results in Figure 4 are made, with the exception that now we assume perfect frequency synchronization in order to concentrate on the performance impact of varying the transmit/receive timing error, τ. A positive value of τ means that the OFDM symbol boundary at the receiver is late with respect to the actual symbol boundary, and therefore inevitably there will be ISI from the next OFDM symbol. A negative value of τ advances the OFDM symbol boundary, but since the CP is preceding the OFDM symbol, the actual effect is equivalent to that of a shortened CP. Unlike the frequency errors, the performance degradation for a positive timing error may be quite abrupt, as seen in Figure 2. The performance degradation of a negative timing error is much more graceful, as it is equivalent to a shortened CP.

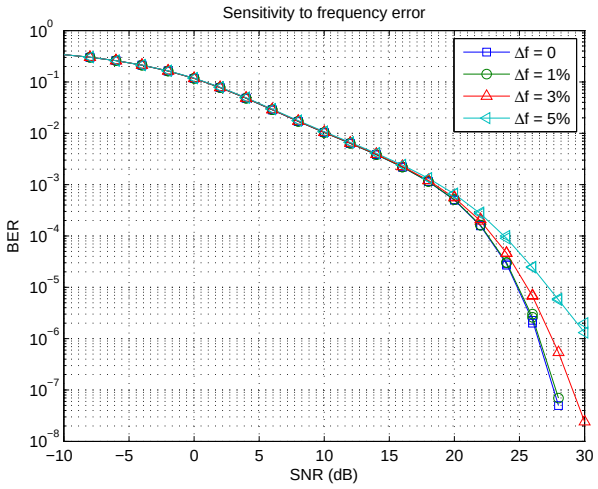

Figure 1:

3 Channel Estimation for Non-Ideal OFDM Systems

The performance characterizations in this section will use two extremes in terms of channel delay spread, namely channel model 1 (CM1), based on (0-4m) line-of-sight (LOS) channel measurements, and channel model 4 (CM4), generated to fit a $25ns$ RMS delay to represent the extreme NLOS multipath channel for UWB applications.

All the evaluations assume an OFDM-based UWB system with $N = 128$ subcarriers with a subcarrier spacing of $4.125MHz$ ($T = 242.42ns$). The CP duration is assumed to be $T_{CP} = 60.61ns$, and we assume a single-tap equalizer detector. The BERs shown are the result of averaging the performance over 1000 channel realizations. Analytical results are compared to simulation results for all the evaluations (simulation results are distinguished by characters in the plots e.g., '*' and analyses by corresponding solid lines).

Figures 3 through 6 show the BER sensitivity to the pilot signal density. For these evaluations, we assume 1% residual frequency error and an early sampling at the receiver corresponding to 12.5% of the CP, i.e., $\tau = -4T_c$. Figure 3 shows the BER averaged over 1000 CM1 realizations for different pilot densities for the frequency domain - least squares (FD-LS) channel estimator. The BER is shown for perfect channel estimation, for a TDM pilot (100% pilot density) and for FDM pilots with 50%, 33% and 25% densities. Results for TDM pilots assume the channel remains constant for a time interval starting at the OFDM symbol used for channel estimation and ending at the last OFDM symbol used for data detection. The FD-LS channel estimates for the FDM pilot cases are linearly interpolated to obtain the channel estimates on the data subcarriers. As we can see, the performance worsens as we go to sparser pilot densities.

Figure 4 shows the same characterization for a DFT-based channel estimator. The number of time-domain samples to obtain the estimate has been set to $N_h = 64$ for both the TDM pilot and the FDM pilot with 50% density. The number of time-domain samples has been set to the number of pilot subcarriers for the other FDM pilot configurations, i.e., $N_h = 43$ and $N_h = 32$ for 33%

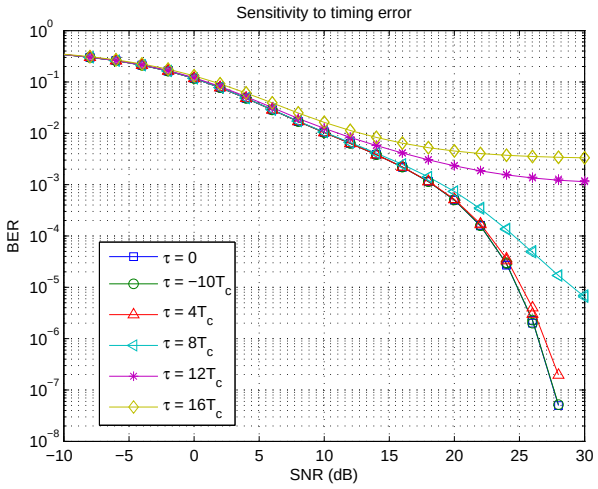

Figure 2:

and 25% pilot densities, respectively. The performance improvement with respect to the FD-LS channel estimator is significant, particularly for the FDM pilots with sparser densities.

Figure 5 shows the average performance of the FD-LS channel estimator using 1000 CM4 realizations. This channel model incurs high levels of ISI, and from the results, we can see that there is now a large degradation due to channel estimation. Indeed, the BER for the FDM pilot hits an error floor at very large values. Therefore, these results indicate that the linear interpolator that we use in conjunction with the FD-LS channel estimator is not adequate for this highly frequency selective channel. Also, we can clearly see the very severe impact of ISI into the detection performance.

Figure 6, in turn, shows the same performance characterization for a DFT-based channel estimator. The number of time-domain samples to obtain the estimate has been set in the same way as for Figure 4, i.e., $N_h = 64$ for the TDM pilot and the FDM pilot with 50% density, and $N_h = 43$ and $N_h = 32$ for the 33% and 25% pilot densities, respectively. Note that $N_h = 64$ corresponds to twice the time span of the CP, and this is the case with best BER performance. Further, note that performance of the DFT-based channel estimator is consistently better than that of the FD-LS channel estimator, however the performance degradation due to channel estimation is quite considerable in either case.

4 Sensor Network Relay Placement

An algorithm is given for placing relays at spatial positions to improve the reliability of communicated data in a sensor network. The network consists of many power-limited sensors, a small set of relays, and a receiver. The receiver receives a signal directly from each sensor and also indirectly from one relay per sensor. The relays rebroadcast the transmissions in order to achieve diversity at the receiver. Both amplify-and-forward and decode-and-forward relay networks are considered. Channels are modeled with Rayleigh fading, path loss, and additive white Gaussian

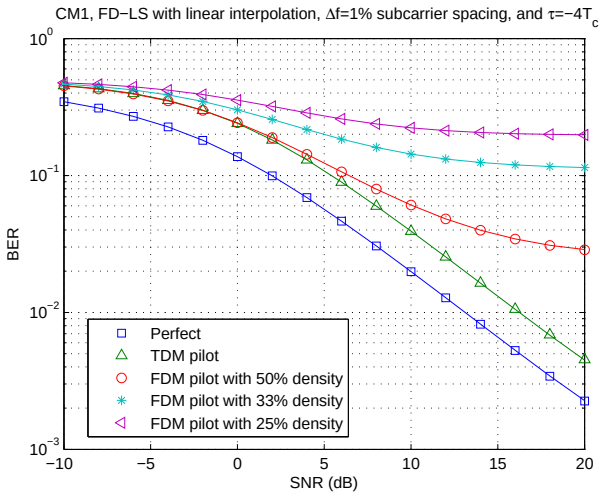

Figure 3:

noise. Performance analysis and numerical results are given.

Wireless sensor networks typically consist of a large number of small, power-limited sensors distributed over a planar geographic area. In some scenarios, the sensors collect information which is transmitted to a single receiver for further analysis. A small number of radio relays with additional processing and communications capabilities can be strategically placed to help improve system performance. Two important problems we consider here are to position the relays and to determine, for each sensor, which relay should rebroadcast its signal.

In this work, we attempt to position the relays and determine which relay should rebroadcast each sensor's transmissions in order to minimize the average probability of error. We use a more elaborate communications model which includes path loss, fading, additive white Gaussian noise, and diversity. We use a network model in which all relays either use amplify-and-forward or decode-and-forward communications. Each sensor in the network transmits information to the receiver both directly and through a single-hop relay path. The receiver uses the two received signals to achieve diversity. Sensors identify themselves in transmissions and relays know for which sensors they are responsible. We assume TDMA communications by sensors and relays so that there is (ideally) no transmission interference. While such interference, due to effects such as multipath and imperfect frame synchronization, can be incorporated into our model, it is out of the scope of this work.

We present an algorithm that determines relay placement and assigns each sensor to a relay. We refer to this algorithm as the *relay placement algorithm*. The algorithm has some similarity to the Lloyd algorithm. We describe geometrically, with respect to fixed relay positions, the sets of locations in the plane in which sensors are (optimally) assigned to the same relay, and give performance results based on these analyses and using numerical computations.

In a sensor network, we refer to sensors, relays, and the receiver as *nodes*. We assume that transmission of $b_i \in \{-1, 1\}$ by node i uses the binary phase shift keyed (BPSK) signal $s_i(t)$, and we denote the transmission energy per bit by E_i. In particular, we assume all sensor nodes

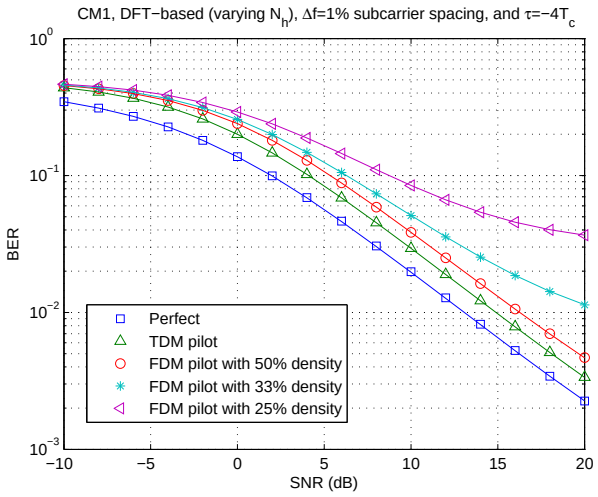

Figure 4:

transmit at the same energy per bit, denoted by E_{Tx}. The communications channel model includes path loss, additive white Gaussian noise (AWGN), and fading. Let $L_{i,j}$ denote the far field path loss between two nodes i and j that are separated by a distance $d_{i,j}$ (in meters). We consider the free-space law model for which[1]

$$L_{i,j} = \frac{F_2}{d_{i,j}^2} \tag{3}$$

where:

$F_2 = \frac{\lambda^2}{16\pi^2}$ (in meters^2)
$\lambda = c/f_0$ is the wavelength of the carrier wave (in meters)
$c = 3 \cdot 10^8$ is the speed of light (in meters/second)
f_0 is the frequency of the carrier wave (in Hz).

We define a *sensor network with relays* to be a collection of sensors and relays in $\mathbb{R}^2$, together with a single receiver at the origin, where each sensor transmits to the receiver both directly and through some predesignated relay for the sensor, and the system performance is evaluated using the measure given in (4). Specifically, let $\mathbf{x}_1, \ldots, \mathbf{x}_M \in \mathbb{R}^2$ be the sensor positions and let $\mathbf{y}_1, \ldots, \mathbf{y}_N \in \mathbb{R}^2$ be the relay positions. Typically, $N \ll M$. Let

$$p : \mathbb{R}^2 \to \{1, \ldots, N\}$$

be a *sensor-relay assignment*, where $p(\mathbf{x}) = i$ means that if a sensor were located at position $\mathbf{x}$, then it would be assigned to relay $\mathbf{y}_i$. Let $\mathcal{S}$ be a bounded subset of $\mathbb{R}^2$. Throughout this section

[1]Much of the material of this work can be generalized by replacing the path loss exponent 2 by any positive, even integer, and F_2 by a corresponding constant.

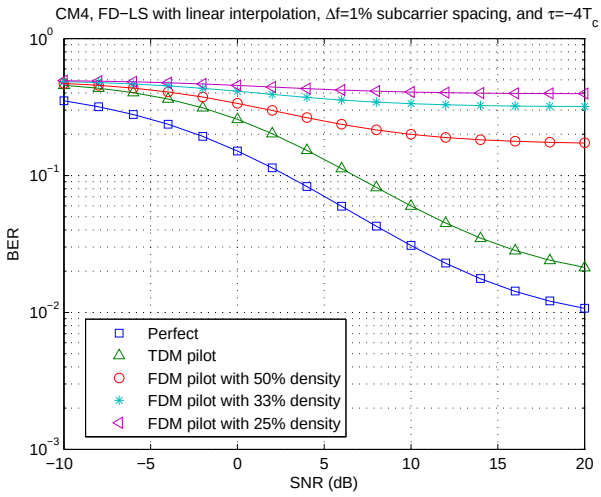

Figure 5:

we will consider sensor-relay assignments whose domains are restricted to $\mathcal{S}$ (since the number of sensors is finite). Let the *sensor-averaged probability of error* be given by

$$\frac{1}{M}\sum_{s=1}^{M} P_e^{(\mathbf{x}_s, p(\mathbf{x}_s), \mathrm{Rx})}. \tag{4}$$

Note that (4) depends on the relay locations through the sensor-relay assignment p.

The proposed iterative algorithm attempts to minimize the sensor-averaged probability of error[2] over all choices of relay positions $\mathbf{y}_1, \ldots, \mathbf{y}_N$ and sensor-relay assignments p. The algorithm operates in two phases. First, the relay positions are fixed and the best sensor-relay assignment is determined; second, the sensor-relay assignment is fixed and the best relay positions are determined. An initial placement of the relays is made either randomly or using some heuristic. The two phases are repeated until the quantity in (4) has converged within some threshold.

In the first phase, we assume the relay positions $\mathbf{y}_1, \ldots, \mathbf{y}_N$ are fixed and choose an optimal[3] sensor-relay assignment p^*, in the sense of minimizing (4). This choice can be made using an exhaustive search in which all possible sensor-relay assignments are examined. A sensor-relay assignment induces a partition of $\mathcal{S}$ into subsets for which all sensors in any such subset are assigned to the same relay. For each relay $\mathbf{y}_i$, let σ_i be the set of all points $\mathbf{x} \in \mathcal{S}$ such that if a sensor were located at position $\mathbf{x}$, then the optimally assigned relay that rebroadcasts its transmissions would be $\mathbf{y}_i$, i.e.,

$$\sigma_i = \left\{\mathbf{x} \in \mathcal{S} : p^*(\mathbf{x}) = i\right\}.$$

We call σ_i the i^{th} *optimal sensor region* (with respect to the fixed relay positions).

[2]Here we minimize (4); however, the algorithm can be adapted to minimize other performance measures.

[3]This choice may not be unique, but we select one such minimizing assignment here. Also, optimality of p^* here depends only on the values $p^*(\mathbf{x}_1), \ldots, p^*(\mathbf{x}_M)$.

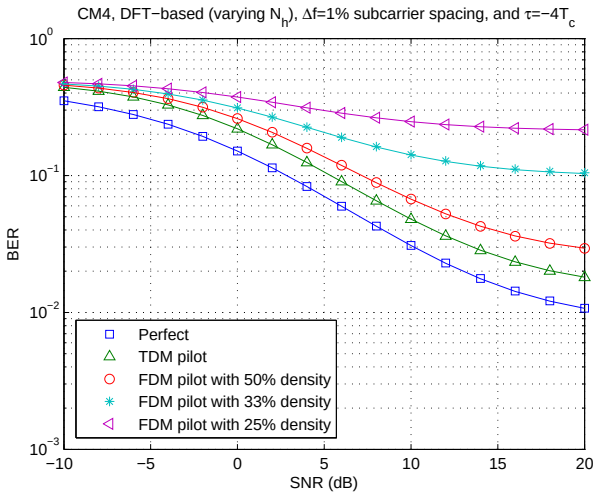

Figure 6:

In the second phase, we assume the sensor-relay assignment is fixed and choose optimal[4] relay positions in the sense of minimizing (4). Numerical techniques can be used to determine such optimal relay positions. For the first three invocations of phase 2 in the iterative algorithm, we used an efficient (but slightly sub-optimal) numerical approach that quantizes a bounded subset of $\mathbb{R}^2$ into gridpoints. For a given relay, the best gridpoint was selected as the new location for the relay. For subsequent invocations of phase 2, the restriction of lying on a gridpoint was removed and a steepest descent technique was used to refine the relay locations.

We now geometrically describe the optimal sensor regions used in Phase 1 of the algorithm by considering specific relay protocols and channel models. In particular, we examine amplify-and-forward and decode-and-forward relaying protocols in conjunction with either AWGN channels or Rayleigh fading channels. We define the *internal boundary* of any optimal sensor region σ_i to be the portion of the boundary of σ_i that does not lie on the boundary of $\mathcal{S}$. For amplify-and-forward and AWGN channels, we show that the internal boundary of each optimal sensor region consists only of circular arcs. For the other three combinations of relay protocol and channel type, we show that as the transmission energies of sensors and relays grow, the internal boundary of each optimal sensor region converges to finite combinations of circular arcs and/or line segments.

In particular, we have the following four key results:

Theorem 4.1. *Consider a sensor network with amplify-and-forward relays and AWGN channels. Then, the internal boundary of each optimal sensor region consists of circular arcs.*

Theorem 4.2. *Consider a sensor network with decode-and-forward relays and AWGN channels, and, for all relays i, let $E_i/N_0 \to \infty$ and $E_{\mathrm{Tx}}/N_0 \to \infty$ such that $(E_i/N_0)/(E_{\mathrm{Tx}}/N_0)$ has a limit. Then, the internal boundary of each optimal sensor region consists asymptotically of circular arcs and line segments.*

[4]This choice may not be unique, but we select one such set of positions here.

Theorem 4.3. *Consider a sensor network with amplify-and-forward relays and Rayleigh fading channels, and let* $E_{\mathrm{Tx}}/N_0 \to \infty$*. Then, each optimal sensor region is asymptotically equal to the corresponding relay's nearest-neighbor region.*

Theorem 4.4. *Consider a sensor network with decode-and-forward relays and Rayleigh fading channels, and, for all relays* i*, let* $E_i/N_0 \to \infty$ *and* $E_{\mathrm{Tx}}/N_0 \to \infty$ *such that* $(E_i/N_0)/(E_{\mathrm{Tx}}/N_0)$ *has a limit. Then, the internal boundary of each optimal sensor region is asymptotically piecewise linear.*